ARL-CR-0807● Nov 2016

US Army Research Laboratory

Development and Evaluation of a Dynamic, 3-Degree-of-Freedom (DOF) Wind Tunnel Model

prepared by Bryant P Nelson
Bennett Aerospace
107 Kilmayne Dr. No. 137
Cary, NC

under contract W911-QX-14-C-0016

NOTICES

Disclaimers

The findings in this report are not to be construed as an official Department of the Army position unless so designated by other authorized documents.

Citation of manufacturer's or trade names does not constitute an official endorsement or approval of the use thereof.

Destroy this report when it is no longer needed. Do not return it to the originator.

ARL-CR-0807 ● NOV 2016

US Army Research Laboratory

Development and Evaluation of a Dynamic, 3-Degree-of-Freedom (DOF) Wind Tunnel Model

prepared by Bryant P Nelson
Bennett Aerospace
107 Kilmayne Dr. No. 137
Cary, NC

under contract W911-QX-14-C-0016

REPORT DOCUMENTATION PAGE

Form Approved
OMB No. 0704-0188

1. REPORT DATE *(DD-MM-YYYY)*	2. REPORT TYPE	3. DATES COVERED (From - To)
November 2016	Contractor Report	November 2014–October 2015

4. TITLE AND SUBTITLE
Development and Evaluation of a Dynamic, 3-Degree-of-Freedom (DOF) Wind Tunnel Model

5a. CONTRACT NUMBER
W911-QX-14-C-0016

5b. GRANT NUMBER

5c. PROGRAM ELEMENT NUMBER

6. AUTHOR(S)
Bryant P Nelson

5d. PROJECT NUMBER
622618H80RK16

5e. TASK NUMBER

5f. WORK UNIT NUMBER

7. PERFORMING ORGANIZATION NAME(S) AND ADDRESS(ES)
Bennett Aerospace
107 Kilmayne Dr. No. 137
Cary, NC 27511

8. PERFORMING ORGANIZATION REPORT NUMBER
ARL-CR-0807

9. SPONSORING/MONITORING AGENCY NAME(S) AND ADDRESS(ES)
US Army Research Laboratory
ATTN: RDRL-WML-F
Aberdeen Proving Ground, MD 21005-5069

10. SPONSOR/MONITOR'S ACRONYM(S)

11. SPONSOR/MONITOR'S REPORT NUMBER(S)

12. DISTRIBUTION/AVAILABILITY STATEMENT
Approved for public release; distribution is unlimited.

13. SUPPLEMENTARY NOTES

14. ABSTRACT
Wind tunnel experiments have been used for decades to collect data and build representative aerodynamic models; however, the model itself is usually static. This report focuses on the unique design of a dynamic, 3-degree-of-freedom (DOF) wind tunnel model, release mechanism, and sting that is capable of simulating "free-flight" of an 83-mm projectile using its own, self-contained electronics and maneuver mechanisms. The objective is to validate state estimation and control algorithms, parameterize and quantify flight behavior, and assess the performance of the Control Actuation System (CAS). One of the unique aspects is the internal gimbal mechanism, which eliminates any gimbal-induced flow disturbances. All 3 axes can be locked independently and are instrumented with high-resolution feedback. Experiments were conducted at Mach 0.2 and 0.6 in a subsonic and transonic wind tunnel, respectively. Tunnel-specific differences in the sting and release mechanism are highlighted as well as a few representative data sets.

15. SUBJECT TERMS
dynamic wind tunnel, finite element analysis, projectile control, machine design, fluid dynamics

16. SECURITY CLASSIFICATION OF:			17. LIMITATION OF ABSTRACT	18. NUMBER OF PAGES	19a. NAME OF RESPONSIBLE PERSON
a. REPORT	b. ABSTRACT	c. THIS PAGE			Bryant P Nelson
Unclassified	Unclassified	Unclassified	UU	36	19b. TELEPHONE NUMBER (Include area code) 410-306-1211

Contents

List of Figures

List of Tables

Acknowledgments

I would like to acknowledge Ilmars Celmins for his modeling and design support. I would also like to acknowledge the principle investigator Frank Fresconi as well as Jim Maley for establishing requirements and collecting and processing the data we need to further our mission. A special thanks goes out to the wind tunnel operators of the Smoke and Target Defeat Branch of Edgewood Chemical and Biological Center for their patience and assistance.

1. Introduction

Recent military engagements have shown the need for precision strike capability in GPS-denied environments especially at the squad level and against moving targets. To address these challenges the US Army Research Laboratory (ARL) has invested in enabling technologies such as vision-based navigation and high-maneuverability airframes. ARL is designing an 83-mm demonstrator vehicle as a platform to develop and evaluate these technologies and algorithms on precision-guided munitions. As part of this mission, a series of subsonic and transonic wind tunnel experiments were conducted to validate state estimation and control algorithms, parameterize and quantify flight behavior, and assess the performance of the Control Actuation System (CAS). This report focuses on the design and implementation of the dynamic, 3-degree-of-freedom (DOF) wind tunnel model and sting that enabled these experiments.

Dynamic wind tunnel experiments have been conducted for decades, however, most of these experiments use external forces to drive and position a sting-fixed model. These vary from simple rolling stings[1] to stings with elastic elements[2,3] to 1-DOF driven models,[4,5] 2-DOF driven models,[6] and 3-DOF driven models.[7] Some dynamic tunnel experiments do not rely on stings at all. A notable example is a 5-DOF cable-driven, forced-oscillation apparatus used in the National Aeronautics and Space Administration (NASA) Langley Research Center's transonic dynamics tunnel.[8] One of the most sophisticated positioning systems currently available is the 6-DOF parallel kinematic model position mechanism operated by German-Dutch Wind Tunnels.[9] This mechanism has been used successfully on a variety of programs.[10–13]

Few experiments have been done using freely moving models without mechanical constraints. Rajamurthy conducted 1-DOF pitch experiments at low subsonic velocities and collected pitch data via a potentiometer.[14] In contrast to forced oscillations, this model maneuvered itself using onboard servos that controlled the elevons. Gnemmi and Rey conducted supersonic 1-DOF pitch experiments using a projectile that was released via a piston actuator. Angle-of-Attack (AoA) was measured via high-speed video imagery. Pitch damping as well as the pitch effect of the projectiles' plasma actuators were investigated.[15] While these are similar to what we want to accomplish, they are incredibly limited for our purposes given our goals.

The goals of this project are to create a dynamic model capable of the following:

- Three rotational DOF

- Ability to independently lock each DOF
- Onboard feedback on all axes
- Approximately 0.1° resolution on all feedback mechanisms
- Send feedback data to the Guidance Electronics Unit (GEU)
- Model motion driven by GEU-controlled CAS
- Onboard data recording and/or telemetry
- Controlled model release at several fixed AoA and roll positions
- Minimize impact of sting and model release on projectile dynamics
- Robust and reliable performance

Researchers at the French–German Research Institute of Saint–Louis (ISL) are investigating similar guided projectiles' airframes, guidance techniques, and dynamic, model-driven wind tunnel experiments.[16–18] The experimental fixture is very similar to the fixture detailed here and meets many of the listed goals, but differs in a couple of key aspects—primarily the 3-DOF gimbal design and operating velocity. ISL opted for an external gimbal assembly (see Fig. 2 in Section 3) and are testing at an order-of-magnitude lower velocity; however, we share the experimental objectives listed previously.

2. Overview

A wind tunnel model was created that accomplished these goals. The design consisted of 3 main components, a CAS section containing 4 independently controlled canards, an instrumented midbody control section with a GEU and 3-DOF gimbal assembly, and a tail section with an internal translating mass for balancing (Fig. 1). Due to the unique nature of this experiment, subsonic wind tunnel experiments were planned in 2 separate wind tunnels, a continuous-flow subsonic tunnel and a blow-down transonic wind tunnel. The subsonic tunnel was used for initial system performance evaluation at lower loading conditions as well as direct force and moment measurements. The transonic tunnel was operated at high subsonic velocities, which is representative of the flight environment. Two release mechanisms were designed, one for each tunnel. Three stings were designed: one for the transonic tunnel, one for the subsonic tunnel without a force-moment balance, and one incorporating a balance.

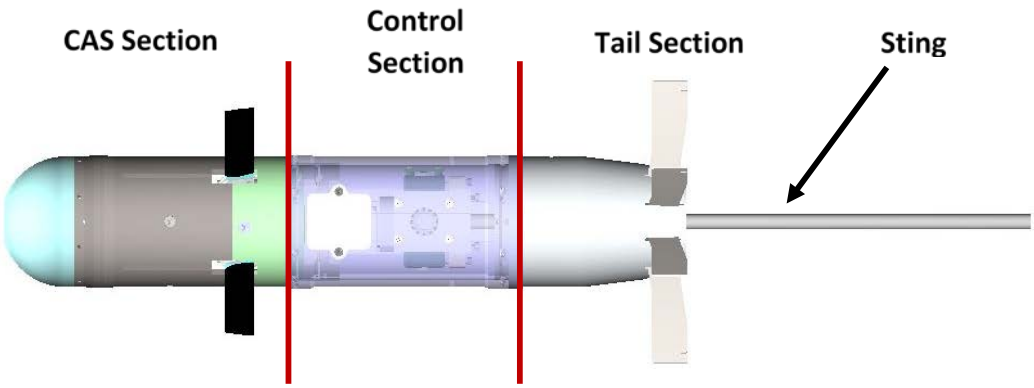

Fig. 1 Full wind tunnel model assembly with subsonic sting

3. Gimbal Assembly

When designing the model, the first major consideration was the best way to implement a 3-DOF sting. The 3-DOF gimbal assembly could be either inside or outside the test article (Fig. 2). Both options have their own advantages and disadvantages. An external 3-DOF assembly would be able to achieve larger deflection angles and would be easier to construct and instrument with feedback. However, the gimbal cage support structure will disrupt the flow around the test article as well as add substantial inertia to the system. Increasing the size of the external cage can minimizes the flow effects of the support structure, but increases the inertia and stresses. If the gimbal cage assembly is inside the test article, then it would not obstruct the flow. Instead, the main drawback would be space constraints and maximum total AoA due to body-sting interference. An internal gimbal assembly was selected because minimizing inertia changes and flow perturbations were weighted more heavily than ease of construction and larger AoA potential.

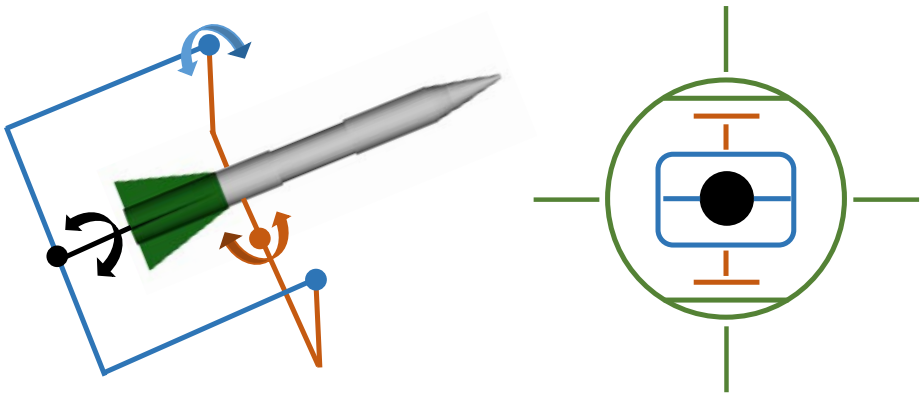

Fig. 2 External gimbal assembly (left) and internal gimbal assembly (right)

To achieve 3 rotational DOF, the internal gimbal assembly had to isolate the 3-DOF with respect to each other, with the outermost cage fixed to the body (orange) and the innermost cage (black) revolving about the sting as shown in Fig. 2. As discussed, the main challenge with this design was fitting all the necessary components inside the body while leaving space for the test article to maneuver. This rig is designed to slide inside any generic test article. However, the design was geared towards current research projects with properties shown in Table 1.

Table 1 Experimental projectile nominal properties

OD (mm)	ID (mm)	Mass (kg)	CG (mm)	I_{axial} (kg-m^2)	I_{trans} (kg-m^2)	Mach (M)	$Load_{M\ 0.2}$ (N)	$Load_{M\ 0.6}$ (N)
83	71	2.65	264	0.0034	0.0388	0.6	35	100

The nominal inner diameter (ID) presents considerable challenges. The driving design parameters of the 3-DOF gimbal assembly were as follows: bearing/sting diameter, feedback sensors, and locking mechanisms. Increasing the sting diameter permits larger loads at the cost of increasing the sting-body interference, thus decreasing the total achievable AoA. As bearing size increases so does the size of each of the 3 cages, which makes instrumenting each axis with feedback increasingly difficult especially considering that some of the feedback sensor must move with the cage and not interfere with the body. After looking into commercial-off-the-shelf bearing options, a 0.375-inch ID bearing was selected because it gave the best balance between sting stiffness, total AoA, and axis instrumentation for this caliber munition.

After a bearing was selected, survivability and performance of the sting was examined. Estimated loading conditions were provided using simulated data for the maximum subsonic wind tunnel velocity (M 0.2) and at the operating velocity of M 0.6 in the transonic tunnel (Table 1). Section 4 contains a detailed finite element analysis (FEA) study of the various sting designs.

Figure 3 shows the 3-DOF gimbal assembly with the sting and bearings. Instrumenting all 3 axes posed considerable space challenges. The roll axis was trivial compared to instrumenting the yaw and pitch axes because of the available space and the ease of adapting to a cylindrical sting. An AMT10× series quadrature encoder from CUI, Inc., was selected as the roll encoder because of the resolution, small size, flexibility on shaft selection, and robust metal housing. Maximum roll rate was not a driving factor due to the nonrolling airframe being considered; however, the AMT10× series encoder is capable of 125 Hz at maximum resolution. Taking into account both quadrature signals and comparing them improves the resolution by a factor of 4 due to the 90° phase offset between both signals.

The test article is also pitching and yawing and since the roll encoder is fixed to the stationary sting, interference between the encoder, the GEU, and body had to be considered and avoided.

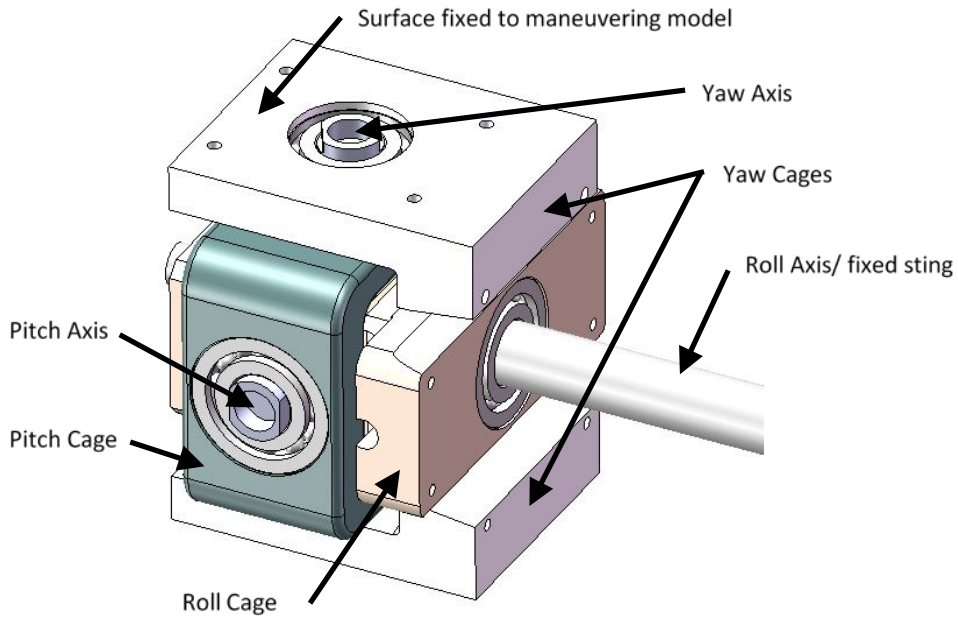

Fig. 3 Three-DOF gimbal assembly

The yaw and pitch feedback sensors had to be low profile to avoid interference which placed substantial limits on the height of the encoder. The only encoders that achieved both the size and resolution goals were magnetic encoder integrated circuits (ICs). An AS5045B absolute magnetic position sensor was selected because it met these requirements. Furthermore, its pulse width modulation output was easily interpreted by the GEU. This encoder required a diametrically magnetized magnet to detect the changes in magnetic flux orientation. The magnets were embedded into the shaft axes as shown in Fig. 4. Custom printed circuit boards were required to mount the IC sensor and position it over the magnet. This sensor only tolerated 0.25 mm of misalignment between the magnetic axis and the AS5045B's magnetic axis. Table 2 shows the encoder properties for the 2 selected encoders.

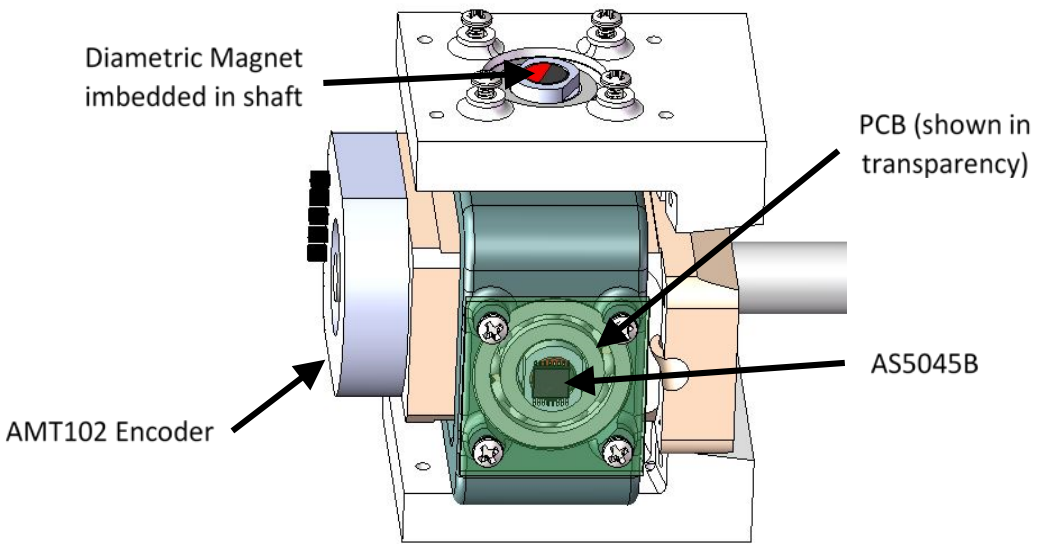

Fig. 4 Gimbal assembly with feedback

Table 2 Encoder properties

Axis	Encoder	Type	Pulses (°/pulse)	Postprocessing counts (°/count)	Form factor (mm)
Roll	AMT102	Capacitive quadrature	2048 (0.176)	8192 (0.044)	28.77 × 43.38 × 9
Yaw/pitch	AS5045B	12-bit magnetic (integrated circuit)	4096 (0.088)	NA	7.8 × 6.2 × 1.86

A method to independently lock each axis with respect to one another was also required. The locking mechanism must cause physical interference between each adjacent cage without obstructing the motion of the other cages around it. More simply, the sting must lock rotation between itself and the roll cage, the roll cage must lock with respect to the pitch cage, and the pitch cage must lock with respect to the yaw cage (Fig. 3). The roll cage was locked to the sting using set screws. They needed to be reinforced by Heli-coil thread insert because the cages were additively manufactured in a glass-fiber reinforced polymer that did not allow sufficient torque to be applied to prevent rolling. Set screws could not be used on the pitch and yaw cages because of interference with the bearings and a lack of support material. Bolts were added that pressed on the aft surface of the pitch cage as shown in Fig. 5. This allowed roll-pitch locking and pitch-yaw locking. Adjusting the depth of the bolts changes the angle between the 2 cages. Using this system, yaw, pitch, or roll can be locked at any angle within the operating range of

±9°. The locking bolts were typically set at 0° or were unscrewed so they did not make contact with the pitch cage to allow unconstrained motion.

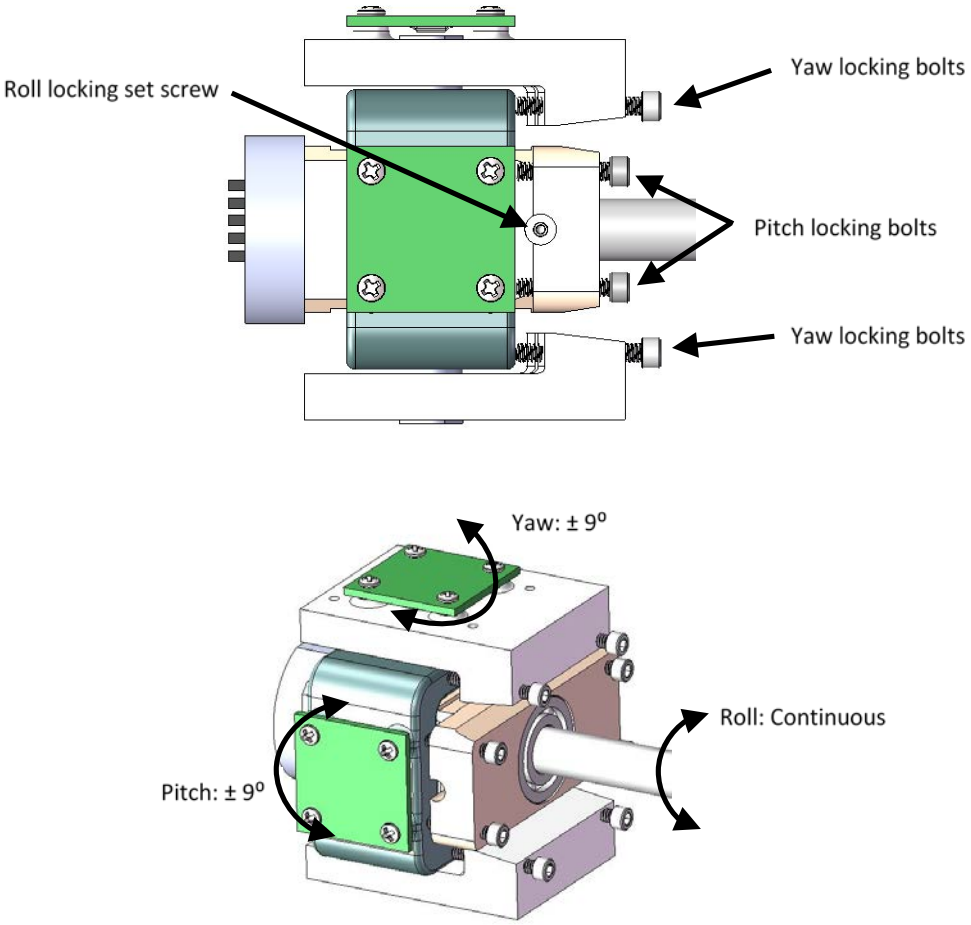

Fig. 5 Gimbal assembly with axis locking mechanisms

The gimbal assembly must be installed inside the test article with the assembly center (the point where roll, pitch, and yaw axes intersect) at the predicted center of gravity (CG) to accurately simulate the movement in free flight (Fig. 6). The axial and transverse moments of inertial as well as the total mass must be as close as possible to the predicted projectile values to get accurate results. A translating steel counterweight was added to the tail to adjust the CG and care was given to ensure the translating mass did not interfere with the sting during maneuvering flight (Fig. 6). The overall weight and moments of inertia were tweaked to within approximately 15% of their theoretical values by adjusting the material thicknesses of additive manufactured parts as well as the mass and location of the counterweight. Actual weight and inertia measurements were performed prior to testing and the results are shown in Table 3.

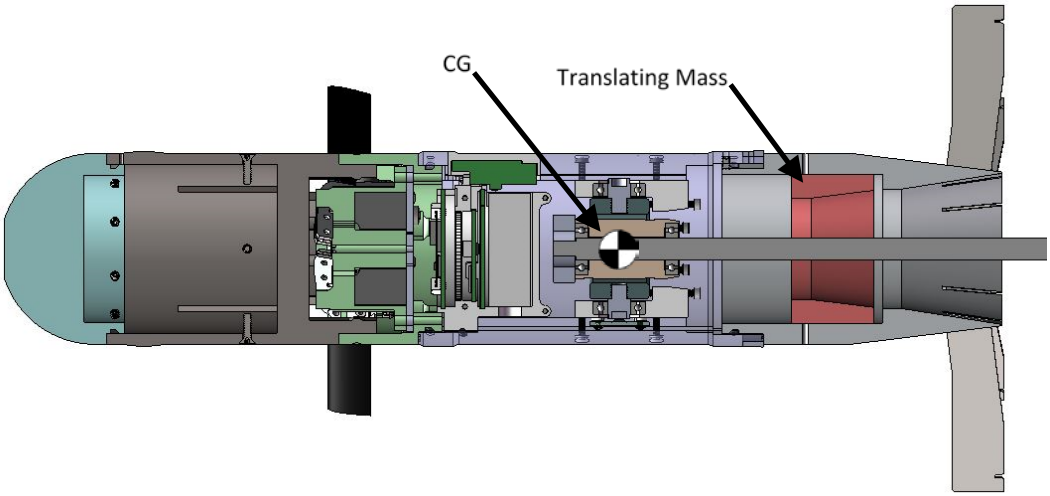

Fig. 6 Cross-sectional view

Table 3 Wind tunnel mass properties compared to nominal mass properties

	OD (mm)	Length (mm)	Mass (kg)	CG (mm)	I_{axial} (kg-m^2)	I_{trans} (kg-m^2)
Nominal	83	427	2.65	264	0.0034	0.0388
WT model	83	429	2.23	266	0.0027	0.0321

Various additive manufacturing methods were used for this project. Stereolithography was used for the GEU board support and the control section body due to the high tolerance of the printed parts. A selective laser sintered glass fiber-reinforced polymer was used for the gimbal assembly, CAS section, and nose section where high strength was required. The control section/CAS support interface proved incapable of tolerating larger loads and both parts have since been traditionally manufactured from aluminum alloy. For further details, Experimental performance is discussed in Section 8.

4. Sting Design

FEA was done to select and qualify sting designs for wind tunnel experiments. One sting was analyzed for use in subsonic wind tunnel experiments and 2 candidate designs were analyzed for use in transonic wind tunnel experiments; a stepped design and a tapered design. All stings shared a common front end interface to the roll encoder and gimbal assembly. Table 1 shows the loading conditions for the subsonic (M 0.2) and transonic (M 0.6) wind tunnels and the load was applied on the bearing surface. To achieve the objective of 9° range of motion, the maximum sting diameter was limited to 0.494 inches, where the tail fins interfere with the sting.

Table 4 and Figs. 7–9 show the inputs and results of FEA analysis on the 3-sting concepts. The subsonic sting was deemed acceptable despite 25-mm deflections because the simulated load is transient and the purpose of the subsonic wind tunnel experiments was to flush out any hardware or software problems and validate control algorithms in a slower, continuous flow wind tunnel. The stepped variant of the transonic wind tunnel sting was selected for use in the transonic tunnel because the tip deflections were 1.3 mm less than the tapered variant with negligible differences in stress.

Table 4 FEA inputs and results

	Material	Load (N)	Yield strength (MPa)	Max stress (MPa)	Peak deflection (mm)
Subsonic sting	17-4 PH	35	1172.1	697.9	25.43
Tapered sting	17-4 PH H900	100	1379.0	431.1	8.587
Stepped sting	17-4 PH H900	100	1379.0	479.8	7.255

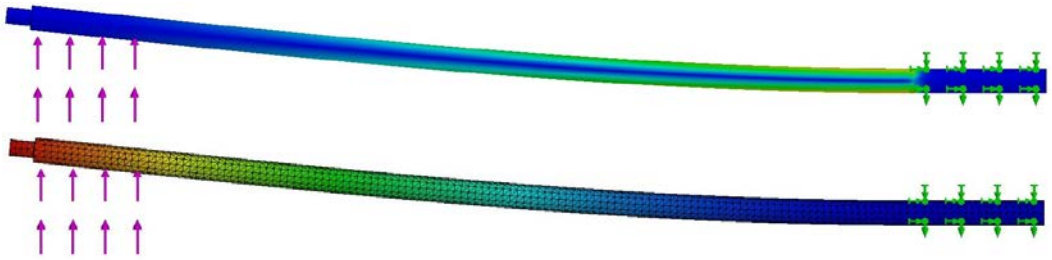

Fig. 7 Subsonic sting: von Mises stress (top) and deflection (bottom)

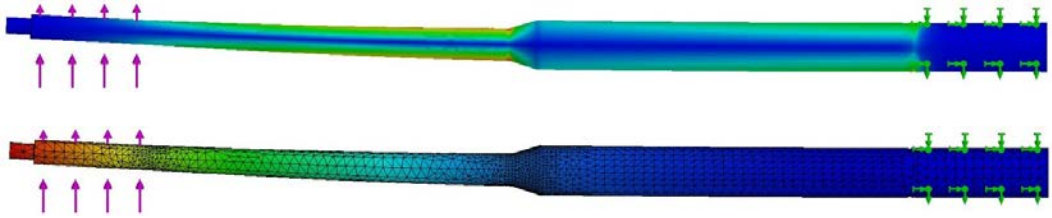

Fig. 8 Transonic tapered sting: von Mises stress (top) and deflection (bottom)

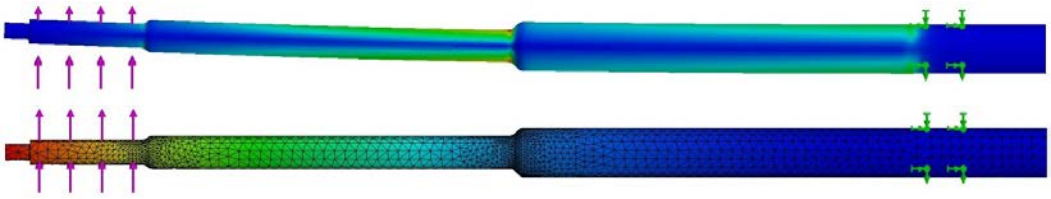

Fig. 9 Transonic stepped sting: von Mises stress (top) and deflection (bottom)

Another sting was designed to support force and moment data collection using a 3/4-inch balance in the subsonic wind tunnel. The objective of these experiments was to directly capture canard forces on the maneuvering body. Ideally, the balance center should be at the CG of the body, but in this case the gimbal assembly occupied that location. The data can be converted from balance coordinates to body coordinates by using the moment arm (distance) from the CG to the balance center. Figure 10 shows a cross-sectional view of the 3-DOF gimbal and the sting-balance assembly. It was important to protect the balance in the event the model was driven to the end of its range. To accomplish this, a tapered section was added to the balance-tunnel adapter to interfere with the tail section prior to balance-tail contact (Fig. 10). This decreased the operating range from ±9° to ±7°.

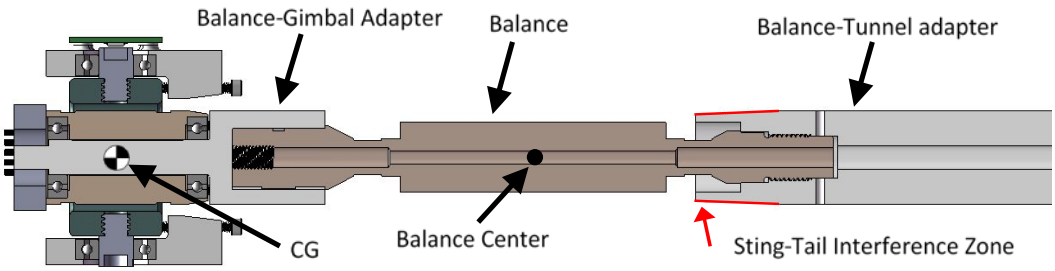

Fig. 10 Cross-sectional view of the gimbal, sting, and balance

5. Release Mechanism Design

A release mechanism is required to release the test article at a known AoA at the proper time while maintaining strong engagement during wind tunnel spin-up. Three release mechanisms were designed for these experiments, 2 variants for the subsonic wind tunnel and 1 for the transonic tunnel. The first series of experiments were conducted in a continuous subsonic wind tunnel; however, this rig prematurely deployed in the transonic wind tunnel due to excessive vibration.

The release mechanism must have a sting-fixed component and an interference component that positions the model. The interference part must not only position the model but also prevent the model rotating with respect to the sting-fixed component. The locking mechanism must be easily and reliably deployed without

excessive force or inducing model motion. A piston release mechanism such as the one used in Strub et al.[15] could work for these experiments but the cost, complexity, and time to implement made this solution less desirable than the additive manufactured alternatives illustrated in Figs. 11 and 12 (Section 6). A piston release would be more attractive if a stronger engagement force was required and pneumatics equipment was available in-house.

6. Subsonic Wind Tunnel Release Mechanisms

The subsonic model release relied on threaded plungers with an imbedded spring-loaded ball-nose that contacted depressions on the sting-fixed component. The tension between the fixed and free components of the model release could be tailored by adjusting the spring force applied by the ball-nose. This was accomplished by screwing/unscrewing the threaded plunger. Proper tension was important because too little tension and the interference component could vibrate off during tunnel spin up. Too much tension increased the force required by the operator, which could cause the string to break or induce model motion during deployment.

It is crucial that the sting-fixed half of the release mechanism be noncircular to prevent the model and the interference half of the release mechanism from rotating with respect to the sting. Three separate interference components were made corresponding to 0°, 3.5°, and 7° initial body angle. Rotating the interference part 90° allowed switching between initial pitch angle or initial yaw angle.

When deployment was desired, the operator pulled on a string attached to the release mechanism and routed outside the tunnel (Fig. 11). As the fixture moved backwards, the ball-nose plunger left the depression in the sting-fixed component further compressing the springs. Once the interference component cleared the fixed component, aerodynamic forces took over and drove the fixture into the sting support. A foam damper was added to cushion the impact against the sting support. After the deployer was activated, the model was free to move in any unconstrained direction.

Figures 11 and 12 show the 2 variants of this design. The primary difference between the 2 versions is the sting diameter, tail design, and how the fixture holds onto the model. The first version (Fig. 11) was designed for a 0.375-inch-diameter sting and had a small tab that fit into a receptacle on the tail fins. The second version of the release mechanism (Fig. 12) was designed for a 1.0-inch-diameter sting (with balance) and grabbed onto the tail fins. The tail assembly was redesigned after the first series of experiments to accommodate larger AoA.

However, the configuration shown in Fig. 12 was only able to achieve the same ±7° operating range as the earlier design due to interference with the balance highlighted in Fig. 10.

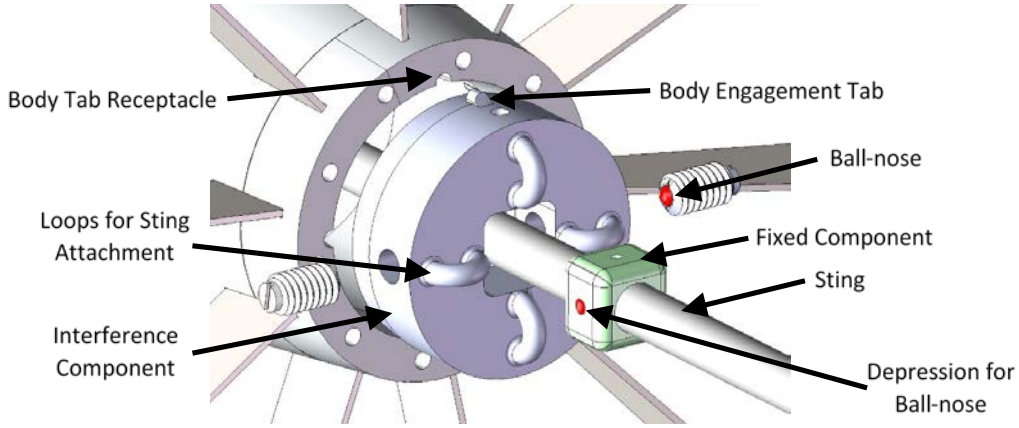

Fig. 11 Exploded view of the subsonic wind tunnel model release

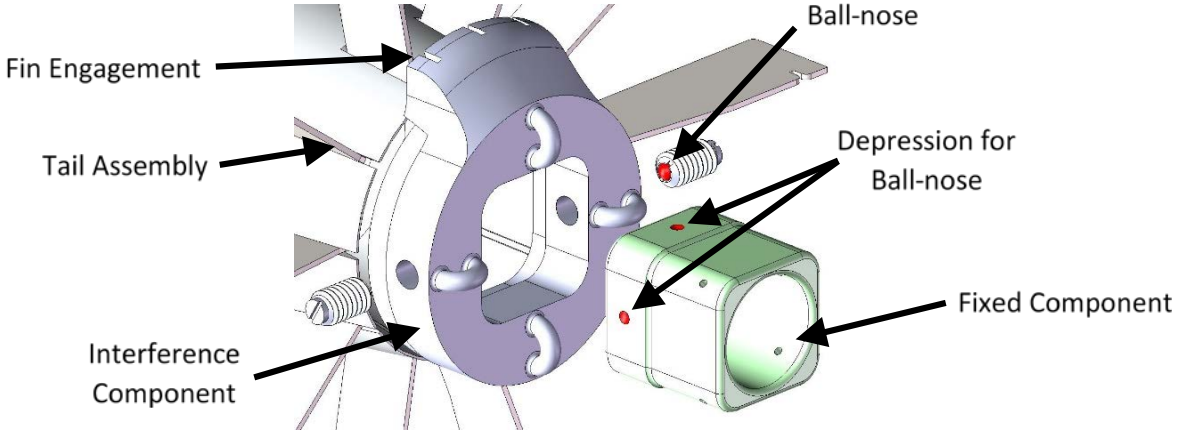

Fig. 12 Exploded view of the subsonic wind tunnel model release, balance configuration

7. Transonic Wind Tunnel Release Mechanisms

The model release for the transonic wind tunnel needed to be more robust than the subsonic version. To meet this objective, the rig needed a better system of engaging and releasing the model. The key difference between the subsonic and transonic tunnels, with regard to the deployment fixture, is the transonic wind tunnel crescent (Fig. 13). The crescent is a component of the transonic wind tunnel and is used to adjust AoA, but was set to 0° AoA for these experiments. The deployment fixture must adapt to and not interfere or damage the crescent. As with the subsonic deployer, the goal of this design was to minimize the flow disturbance caused by

the fixture. Since the crescent already obstructed the flow in the vertical plane, the deployment fixture was designed to be tall and narrow as well. The height was determined by the interference between the crescent and guide rails.

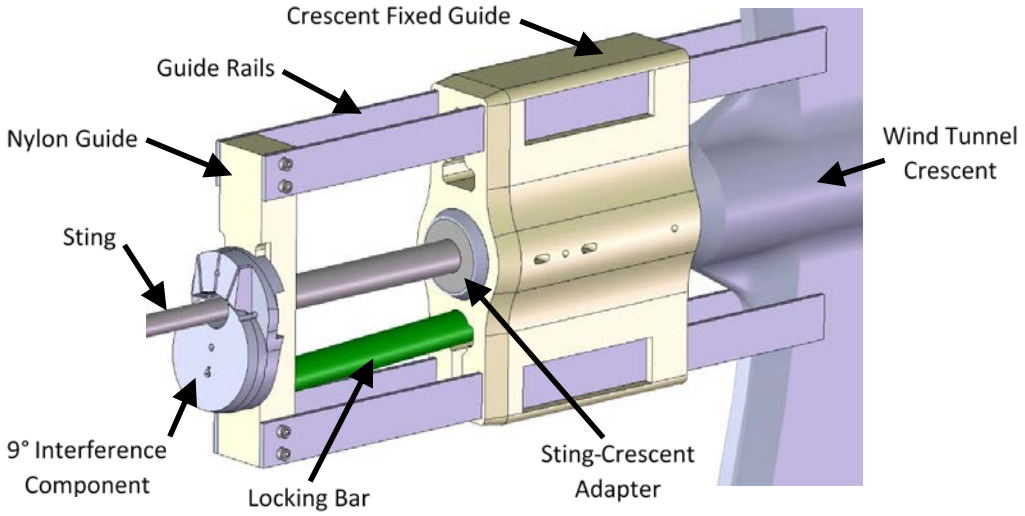

Fig. 13 Exploded view of the subsonic wind tunnel model release, balance configuration

The model release has several components: a crescent-fixed guide, translating interference assembly, 4 metal guide rails, and a locking bar (Fig. 13). The interference assembly consists of the model interference component that bolts onto a nylon guide that slides on the sting and attaches to 4 guide rails. The interference component holds the model predeployment and can be rotated in 90° increments to adjust initial pitch or yaw angles (positive/negative). Three interchangeable interference components were made corresponding to initial body angles of 0°, 4.5°, and 9°, respectively.

The transonic model release relies on a locking bar as its locking mechanism. To lock the model, the translating part of the fixture is moved into position and the interference component engages the model by gripping between the fins identical to Fig. 12. Then the locking bar is pushed upward to wedge itself between the translating and fixed parts of the release mechanism. A string is tied around the locking bar and routed outside the tunnel. When pulled, the locking bar drops down into a slot allowing translation. The 4 guide rails prevent the translating components from rotating relative to the fixed components. Figure 14 shows locked and unlocked views of the release mechanism.

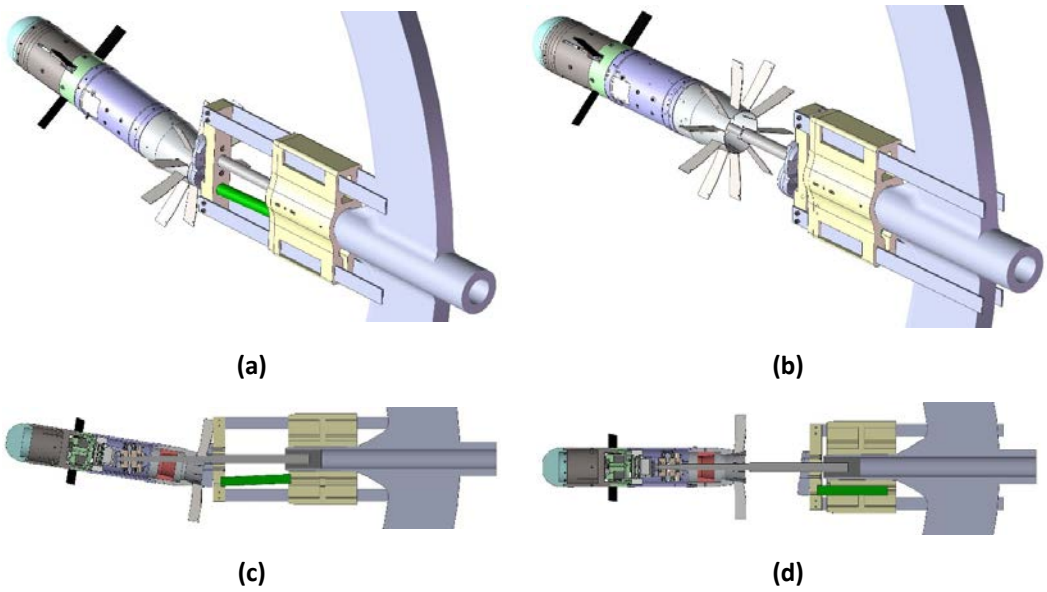

Fig. 14 Isometric view of the a) locked and b) unlocked model; cross-sectional view of the c) locked and d) unlocked model

8. Experimental Performance

Prior to any experiments, aerodynamic roll damping (K_1) and bearing friction (K_2) were estimated using a parameter estimation approach on Eq. 1. A mass of known weight was hung from a string and wrapped around the model in a roll-only configuration such that it provided a constant torque until it separated from the model. Roll encoder data were collected as the model accelerated and decelerated. Given the physical properties of the projectile, the dynamic friction and roll damping coefficients were varied to match the collected data. Figure 15 shows good agreement between the measured and simulated data. The bearing friction is assumed to be the same for the pitch and yaw axes, which is a safe assumption since all axes use the same bearings and all bearings were worn in for 10,000 rotations prior to installation.

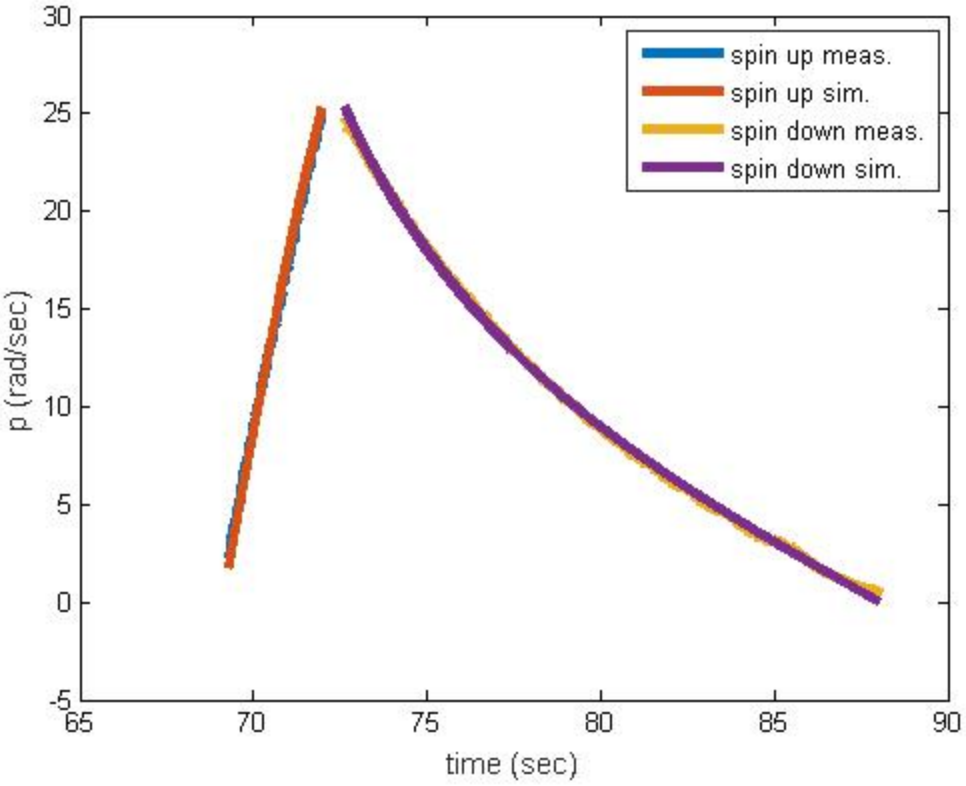

Fig. 15 Bearing friction estimation experiment

$$\dot{p} = \frac{\frac{D}{2}mg - K_1 p^2 - K_2}{I_{xx}} \quad (1)$$

The subsonic wind tunnel experiments were conducted in a continuous flow wind tunnel at Mach 0.2 from 11/13/2014 to 11/25/2014 and 63 runs were completed. Five runs were completed using the instrumented balance (Fig. 10) prior to wind tunnel failure on 6/19/2015. A full test matrix can be found in the Appendix. The model and deployment mechanism functioned as designed and usable data were recorded via telemetry and onboard storage to an SD card. Balance data were collected via LabView. Once all the desired subsonic runs were completed on 11/25/2014, we wanted to move on to the neighboring transonic wind tunnel. However, concern was expressed regarding the survivability of the model on a 0.375-inch-diameter sting. FEA analysis shown in Fig. 7 was only done for subsonic wind tunnel loads. Stress calculations were performed onsite using Eq. 2 for a cantilevered beam with the load estimate in Table 1. While these calculations showed the 17-4 stainless steel sting would not yield under the estimated load, no deflection calculations were performed prior to the transonic run.

$$\sigma_{max} = |M_{max}|\frac{c}{I} = \left|\frac{PL}{Z}\right| \quad (2)$$

The blow-down transonic tunnel was set for Mach 0.6 and resulted in extreme model deflections and balloting. High-speed video imagery in Fig. 16 shows the extent of these deflections. Despite this extreme motion, no apparent damage to the test article, sting, or tunnel was observed. This led to the development of the larger, stiffer sting previously outlined.

Fig. 16 Select high-speed video frames of the subsonic model in the transonic wind tunnel, Run 63

Four runs were done in the transonic tunnel with the larger sting on 6/19/2015. The first 3 runs were roll only and demonstrated open-loop roll control. The model was set in the pitch-only configuration for the last run. The program attempted a series of open-loop pitch commands followed by close-loop pitch control with the goal of 0° pitch angle. Once the program attempted the close-loop portion, the model was driven unstable. After 5 consecutive forceful model-sting impacts, the CAS separated from the model resulting in catastrophic failure (Fig. 17). Following this failure, a metal control section was fabricated to increase the robustness of the transonic fixture to successive sting impacts. The model now has metal interfaces between all joints.

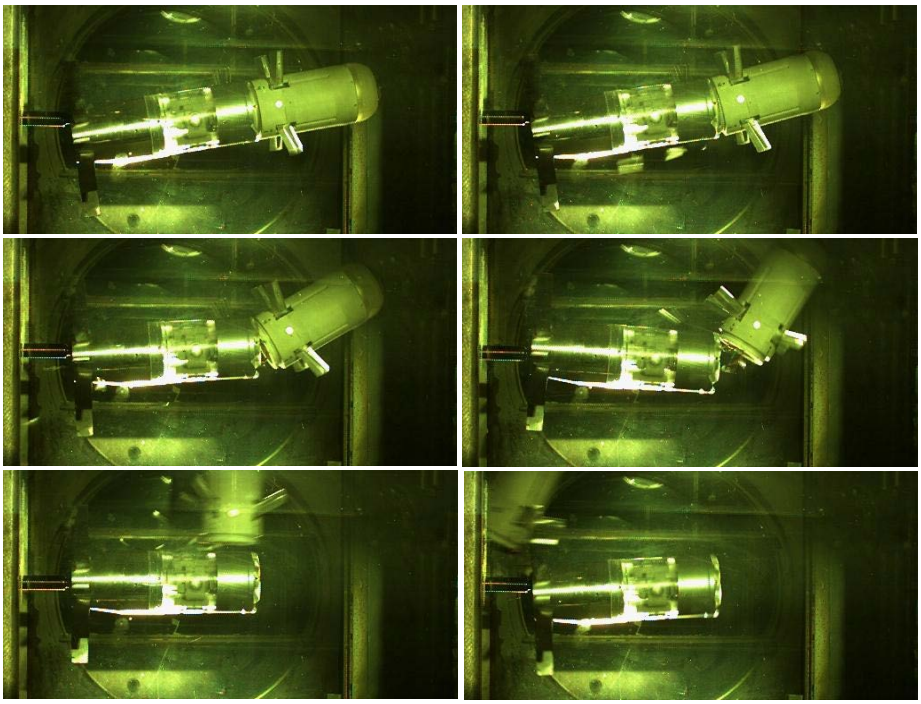

Fig. 17 High-speed video footage of the transonic model failure, Run 72

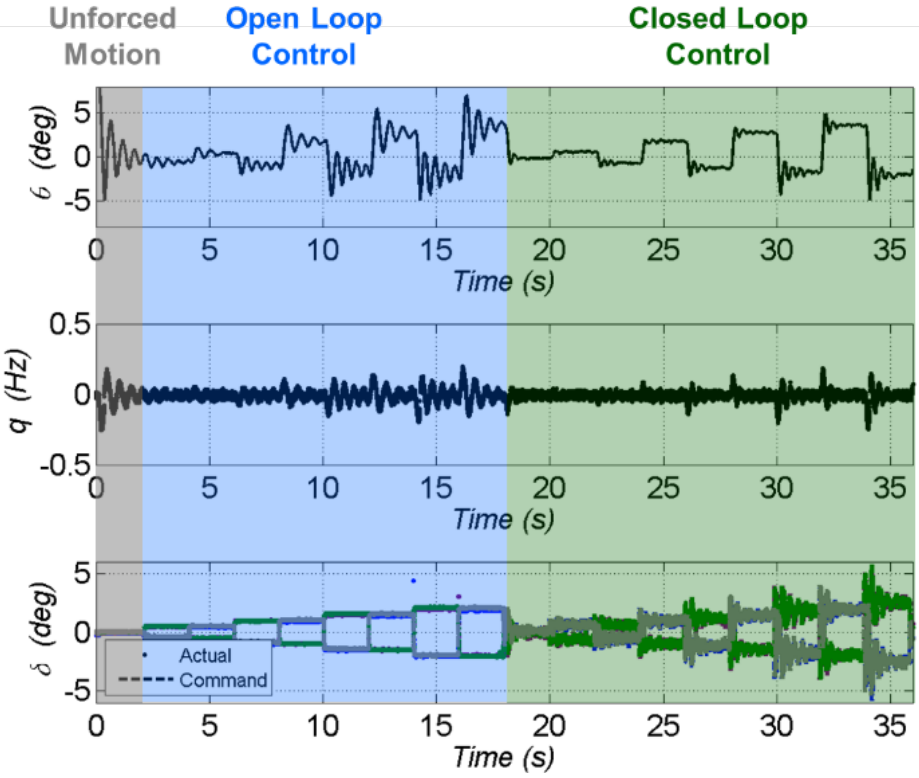

Fig. 18 Sample data from the subsonic wind tunnel experiments

Another series of experiments were conducted in the repaired subsonic wind tunnel and transonic tunnel from 12/7/15 to 12/16/15 with the improved model. Earlier experiments in the subsonic tunnel were repeated with force-moment data collected including full 3-DOF open- and closed-loop controlled experiments. Figure 18 shows a sample data set from a typical run consisting of 3 phases: a free motion section where the model is released from a known angle and allowed to oscillate, an open-loop section where the canards are driven to increasingly larger angles, and a closed-loop section that shows improved performance over the open-loop response. Figure 19 shows the model in the subsonic tunnel with the force-moment balance and drag and normal force data. Specific canard deflection angles that produce dynamic stall oscillations were also investigated in the subsonic tunnel. The plot on the left of Fig. 20 illustrates this phenomenon with the canards at a fixed constant angle and an oscillating body.

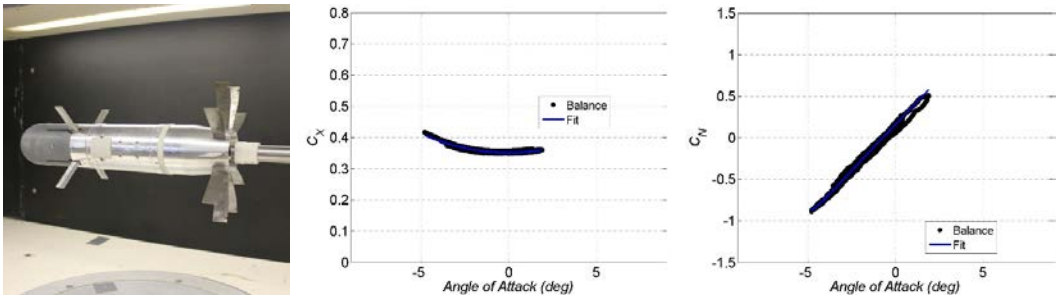

Fig. 19 Three-DOF wind tunnel fixture in the subsonic wind tunnel (left) and balance data from Run 99 (middle, right)

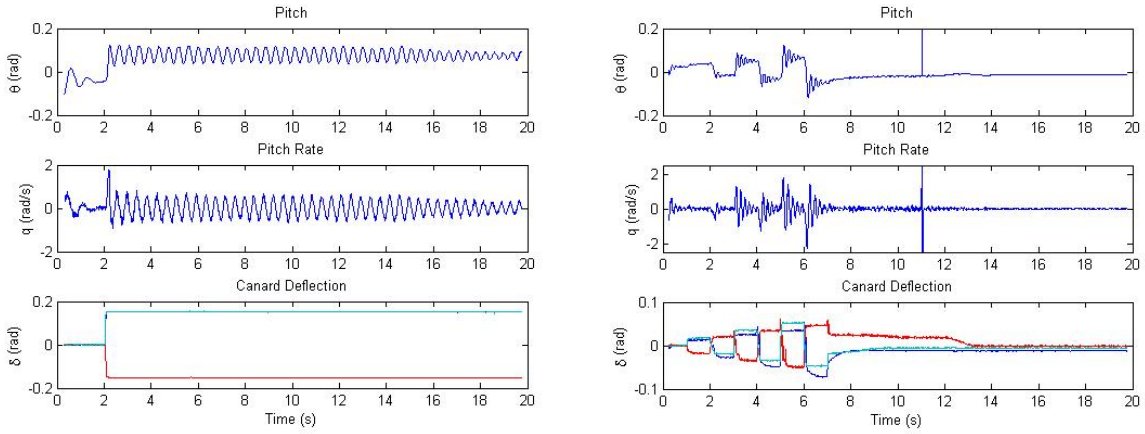

Fig. 20 Subsonic dynamic stall experiment, Run 97 (left); open-loop pitch experiment in the transonic tunnel, Run 105 (right)

Roll only and pitch only experiments were conducted in the transonic wind tunnel during the same timeframe. The changes to the model resulted in a more robust design that was tolerant of model-sting impacts even at higher Mach numbers.

Transonic experiments were used to evaluate different control strategies for mitigating the effect of actuator delay on performance as well as asses CAS performance and state estimation algorithms. The plot on the right of Fig. 20 shows an open-loop pitch response for a typical transonic wind tunnel run.

9. Conclusions and Future Work

Modeling and experimental factors will continue to be analyzed to improve the discrepancies between the model and experiment. One such discrepancy is highlighted in Fig. 21. The 2 types of feedback data collected, high-speed video analysis and encoder data, show good agreement with each other despite being measured from different reference frames (i.e., inertial and body fixed). This suggests the discrepancies between the model and experiment are due to modeling errors, although experimental errors cannot be ruled out completely.

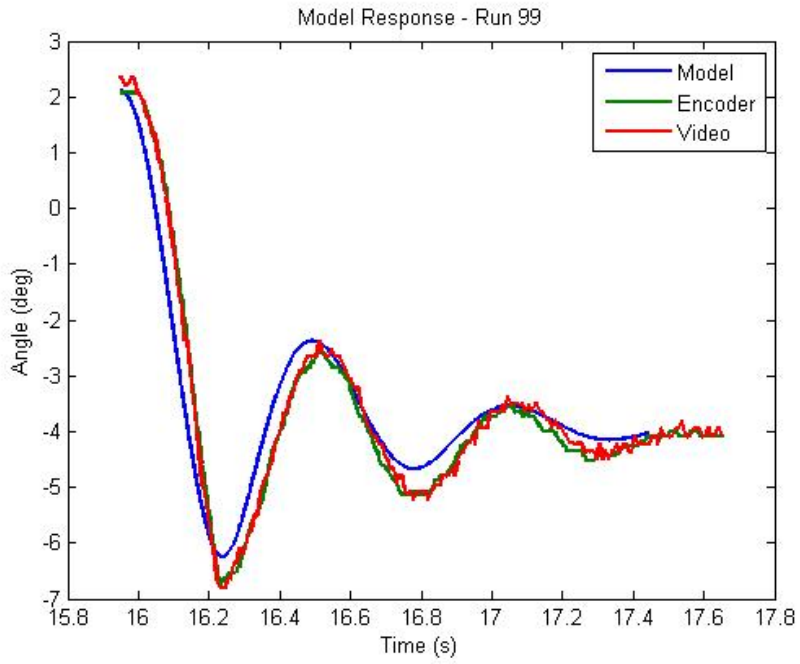

Fig. 21 Model predictions compared to experimental measurements

All the goals established at the outset have been met and represent, to my knowledge, the first model-driven wind tunnel fixture with an internally housed, fully instrumented 3-DOF gimbal. While the models presented in other literature[16–18] are remarkably similar, the gimbals enabling the 3-DOF differ greatly (see Fig. 2). All other requested features have been included, such as onboard data recording, telemetry, controlled model release, and axes agnostic locking capability. This fixture will serve as a useful platform for future experiments with this and other comparable munitions as well as scaled designs.

10. References

1. Pamadi BN, Covell PF, Tartabini PV, Murphy KJ. Aerodynamic characteristics and glide-back performance of langley glide-back booster. In: 22nd Applied Aerodynamics Conference and Exhibit, Providence, RI, 2004.

2. Kabin SV, Kolinko KA, Khrabrov AN, Nushtaev PD. Dynamic test rig and test technique for the aircraft models unsteady aerodynamic characteristics measurements in high subsonic and transonic wind tunnels. In: ICIASF Instrumentation in Aerospace Simulation Facilities, Wright-Patterson AFB, OH, 1995.

3. O'Leary CO. Wind-tunnel measurement of aerodynamic derivatives using flexible-sting rigs. Royal Aircraft Establishment, Bedford, England, 1981.

4. Platou AS, Sternberg J. The magnus characteristics of a 30 mm aircraft bullet. Army Ballistic Research Laboratory (US); Aberdeen Proving Ground (MD): 1956.

5. Carman JB, Hill DW, Christopher JP. Description of captive trajectory store separation testing in the aerodynamic wind tunnel (4T). Arnold Engineering Development Center, Arnold Air Force Station, TN, 1980.

6. Schiff LB, Tobak M. Results from a new wind-tunnel apparatus for studying coning and spinning motions of bodies of revolution. AIAA Journal. 1970;8(11):1953–1957.

7. Murphy PC, Klein V. Validation of methodology for estimating aircraft unsteady aerodynamic parameters from dynamic wind tunnel tests. In: AIAA Atmospheric Flight Mechanics Conference and Exhibit, Austin, TX, 2003.

8. Bennett RM, Farmer MG, Mohr RL, Hall WE Jr. Wind-tunnel technique for determining stability derivatives from cable-mounted models. Journal of Aircraft. 1978; 15(5)304–310.

9. Niedergeschwindigkeits-windkanal braunschweig. Braunschweig (Germany): German-Dutch Wind Tunnels; 2015 Oct 1 [accessed 2015 Oct]. http://www.dnw.aero/Wind-tunnels/NWB.aspx.

10. Loeser T, Bergmann A. Capabilities of deployment tests at DNW-NWB; Meeting paper for US Defence Technical Information Center, DNW German–Dutch Wind Tunnels; 2006.

11. Loeser TD, Vicroy DD, Schutte A. SACCON static wind tunnel tests at DNW-NWB and 14´× 22´ NASA LaRC. In: 28th AIAA Applied Aerodynamics Conference, Chicago, IL, 2010.

12. Cummings RM, Schutte A. An integrated computational/experimental approach to UCAV stability & control estimation: overview of NATO RTO AVT-161. In: 28th AIAA Applied Aerodynamics Conference, Chicago, IL, 2010.

13. Schade N. Simulation of trajectories of cuboid cargos released from a generic transport aircraft. In: 29th AIAA Applied Aerodynamics Conference, Honolulu, HI, 2011.

14. Rajamurthy MS. Generation of comprehensive longitudinal aerodynamic data using dynamic wind-tunnel simulation. Journal of Aircraft. 1997; 34(1): 29–33.

15. Gnemmi P, Rey C. Plasma actuation for the control of a supersonic projectile. Journal of Spacecraft and Rockets. 2009;46(5)989–998.

16. Strub G, Gassmann V, Theodoulis S, Dobre S, Basset, M. Hardware-in-the-loop experimental setup development for a guided projectile in a wind tunnel, in 2014. IEEE/ASME International Conference on Advanced Intelligent Mechatronics (AIM), Besançon, France, 2014.

17. Strub G, Theodoulis S, Gassmann V, Dobre S, Basset M. Pitch axis control for a guided projectile in a wind tunnel hardware-in-the-loop setup. Journal of Spacecraft and Rockets. 2015;52(6):1614–1626.

18. Strub G, Basset, M. Skid-to-turn autopilot design and validation for an experimental guided projectile prototype. In: AIAA Guidance, Navigation, and Control Conference, San Diego, CA, 2016.

INTENTIONALLY LEFT BLANK.

Appendix. Experimental Test Matrix

This appendix appears in its original form, without editorial change.

Run Number	Tunnel & Configuration	Degrees-of-Freedom	Initial Pitch (deg)	Initial Roll Rate (Hz)	Initial Canard Deflection (deg)	Mach	Control
1	Subsonic	Roll Only	0	0	4	0.2	Off
2	Subsonic	Pitch Only	7	0	4	0.2	Off
3	Subsonic	Pitch Only	7	0	4	0.2	Off
4	Subsonic	Roll-Pitch-Yaw	7	0	4	0.2	Off
5	Subsonic	Roll Only	0	0	0	0.2	Open Loop
6	Subsonic	Roll Only	0	1	6	0.2	Closed Loop
7	Subsonic	Roll Only	0	0	0	0.2	Open Loop
8	Subsonic	Roll Only	0	0	0	0.2	Open Loop
9	Subsonic	Roll Only	0	0	0	0.2	Open Loop
10	Subsonic	Roll Only	0	0	0	0.2	Open Loop
11	Subsonic	Roll Only	0	0	0	0.2	Open Loop
12	Subsonic	Roll Only	0	0	0	0.2	Open Loop
13	Subsonic	Roll Only	0	0	0	0.2	Open Loop
14	Subsonic	Roll Only	0	0	0	0.2	Open Loop
15	Subsonic	Roll Only	0	0	0	0.2	Off
16	Subsonic	Pitch Only	7	0	0	0.2	Off
17	Subsonic	Pitch Only	3.5	0	0	0.2	Open Loop
18	Subsonic	Pitch Only	7	0	0	0.2	Open Loop
19	Subsonic	Pitch Only	7	0	0	0.2	Open Loop
20	Subsonic	Pitch Only	7	0	0	0.2	Open Loop
21	Subsonic	Pitch Only	7	0	0	0.2	Open Loop
22	Subsonic	Pitch Only	7	0	0	0.2	Open Loop
23	Subsonic	Pitch Only	3.5	0	0	0.2	Open Loop
24	Subsonic	Pitch Only	3.5	0	0	0.2	Open Loop
25	Subsonic	Pitch Only	3.5	0	0	0.2	Open Loop
26	Subsonic	Roll-Pitch-Yaw	3.5	0	0	0.2	Open Loop
27	Subsonic	Roll-Pitch-Yaw	3.5	0	0	0.2	Open Loop
28	Subsonic	Roll-Pitch-Yaw	3.5	0	0	0.2	Open Loop
29	Subsonic	Roll-Pitch-Yaw	3.5	0	0	0.2	Open Loop
30	Subsonic	Roll-Pitch-Yaw	3.5	0	0	0.2	Open Loop
31	Subsonic	Roll-Pitch-Yaw	3.5	0	0	0.2	Open Loop
32	Subsonic	Roll-Pitch-Yaw	3.5	0	0	0.2	Open Loop
33	Subsonic	Roll-Pitch-Yaw	3.5	0	0	0.2	Open Loop
34	Subsonic	Roll-Pitch-Yaw	3.5	0	0	0.2	Open Loop
35	Subsonic	Roll-Pitch-Yaw	3.5	0	0	0.2	Open Loop
36	Subsonic	Roll-Pitch-Yaw	3.5	0	0	0.2	Open Loop
37	Subsonic	Roll-Pitch-Yaw	3.5	0	0	0.2	Open Loop
38	Subsonic	Roll-Pitch-Yaw	3.5	0	0	0.2	Open Loop
39	Subsonic	Roll-Pitch-Yaw	3.5	0	0	0.2	Open Loop
40	Subsonic	Roll-Pitch-Yaw	3.5	0	0	0.2	Open Loop
41	Subsonic	Roll-Pitch-Yaw	3.5	0	0	0.2	Open Loop
42	Subsonic	Roll-Pitch-Yaw	3.5	0	0	0.2	Open Loop

43	Subsonic	Roll-Pitch-Yaw	3.5	0	0	0.2	Open Loop
44	Subsonic	Roll-Pitch-Yaw	3.5	0	0	0.2	Open Loop
45	Subsonic	Roll-Pitch-Yaw	3.5	0	0	0.2	Open Loop
46	Subsonic	Roll-Pitch-Yaw	3.5	0	0	0.2	Open Loop
47	Subsonic	Pitch Only	7	0	0	0.2	Open Loop
48	Subsonic	Pitch Only	7	0	0	0.2	Open Loop
49	Subsonic	Pitch Only	5.4	0	0	0.2	Open Loop
50	Subsonic	Pitch Only	8.6	0	0	0.2	Open Loop
51	Subsonic	Pitch Only	7	0	0	0.2	Open Loop
52	Subsonic	Pitch Only	7	0	0	0.2	Open Loop
53	Subsonic	Pitch Only	7	0	0	0.2	Open Loop
54	Subsonic	Pitch Only	-7	0	0	0.2	Open Loop
55	Subsonic	Roll Only	0	0	0	0.2	Open Loop
56	Subsonic	Roll Only	0	0	0	0.2	Open Loop
57	Subsonic	Roll Only	0	0	0	0.2	Open Loop
58	Subsonic	Roll-Pitch-Yaw	7	0	0	0.2	Open Loop
59	Subsonic	Roll-Pitch-Yaw	7	0	0	0.2	Open Loop
60	Subsonic	Roll-Pitch-Yaw	7	0	0	0.2	Open Loop
61	Subsonic	Roll Only	7	0	0	0.2	Open Loop
62	Subsonic	Roll Only	0	0	0	0.2	Open Loop
63	Subsonic	Roll Only	7	0	0	0.2	Off
64	Subsonic, balance	Pitch Only	7	0	0	0.2	Open Loop
65	Subsonic, balance	Roll-Pitch-Yaw	7	0	0	0.2	Closed Loop
66	Subsonic, balance	Roll-Pitch-Yaw	7	0	0	0.2	Closed Loop
67	Subsonic, balance	Roll-Pitch-Yaw	7	0	0	0.2	Closed Loop
68	Subsonic, balance	Pitch Only	7	0	0	0.2	Closed Loop
69	Transonic	Roll Only	0	0	0	0.6	Open Loop
70	Transonic	Roll Only	0	0	0	0.6	Open Loop
71	Transonic	Roll Only	0	0	0	0.6	Open Loop
72	Transonic	Pitch Only	9	0	0	0.6	Closed Loop
73	Transonic	Roll Only	0	0	0	0.6	Closed Loop
74	Subsonic, balance	Pitch Only	7	0	0	0.2	Closed Loop
75	Subsonic, balance	Pitch Only	7	0	0	0.2	Closed Loop
76	Subsonic, balance	Pitch Only	7	0	0	0.2	Closed Loop
77	Subsonic, balance	Pitch Only	7	0	0	0.2	Closed Loop
78	Subsonic, balance	Pitch Only	7	0	0	0.2	Closed Loop
79	Subsonic, balance	Pitch Only	7	0	0	0.2	Closed Loop
80	Subsonic, balance	Pitch Only	7	0	0	0.2	Closed Loop
81	Subsonic, balance	Yaw Only	7	0	0	0.2	Closed Loop
82	Subsonic, balance	Yaw Only	7	0	0	0.2	Closed Loop
83	Subsonic, balance	Pitch Only	7	0	0	0.2	Closed Loop
84	Subsonic, balance	Pitch Only	7	0	0	0.2	Closed Loop
85	Subsonic, balance	Pitch Only	7	0	0	0.2	Closed Loop
86	Subsonic, balance	Pitch Only	7	0	0	0.2	Closed Loop
87	Subsonic, balance	Pitch Only	7	0	0	0.2	Closed Loop
88	Subsonic, balance	Pitch Only	7	0	0	0.2	Closed Loop
89	Subsonic, balance	Pitch Only	7	0	0	0.2	Closed Loop
90	Subsonic, balance	Roll Only	0	0	0	0.2	Closed Loop

91	Subsonic, balance	Roll Only	0	0	0	0.2	Closed Loop
92	Subsonic, balance	Roll Only	0	0	0	0.2	Closed Loop
93	Subsonic, balance	Roll-Pitch-Yaw	7	0	0	0.2	Closed Loop
94	Subsonic, balance	Roll-Pitch-Yaw	7	0	0	0.2	Closed Loop
95	Subsonic, balance	Pitch Only	7	0	0	0.2	Closed Loop
96	Subsonic, balance	Pitch Only	7	0	0	0.2	Closed Loop
97	Subsonic, balance	Pitch Only	7	0	0	0.2	Closed Loop
98	Subsonic, balance	Pitch Only	7	0	0	0.2	Closed Loop
99	Subsonic, balance	Pitch Only	7	0	0	0.2	Closed Loop
100	Subsonic, balance	Pitch Only	7	0	0	0.2	Closed Loop
101	Subsonic, balance	Pitch Only	7	0	0	0.2	Closed Loop
102	Subsonic, balance	Pitch Only	7	0	0	0.2	Closed Loop
103	Subsonic, balance	Pitch Only	7	0	0	0.2	Closed Loop
104	Subsonic, balance	Roll-Pitch-Yaw	9	0	0	0.2	Closed Loop
105	Subsonic, balance	Pitch Only	9	0	0	0.2	Closed Loop
106	Subsonic, balance	Pitch Only	9	0	0	0.2	Closed Loop
107	Subsonic, balance	Pitch Only	9	0	0	0.2	Closed Loop
108	Subsonic, balance	Pitch Only	9	0	0	0.2	Closed Loop
109	Subsonic, balance	Pitch Only	9	0	0	0.2	Closed Loop
110	Subsonic, balance	Pitch Only	9	0	0	0.2	Closed Loop
111	Subsonic, balance	Pitch Only	9	0	0	0.2	Closed Loop

List of Symbols, Abbreviations, and Acronyms

AoA	Angle-of-Attack
ARL	US Army Research Laboratory
CAS	Control Actuation System
CG	center of gravity
DOF	degree-of-freedom
FEA	finite element analysis
GEU	Guidance Electronics Unit
GPS	global positioning system
IC	integrated circuit
ID	inner diameter
ISL	French–German Research Institute of Saint–Louis
mm	millimeter
NASA	National Aeronautics and Space Administration
OD	outer diameter
SD	Secure Digital

1 (PDF) DEFENSE TECHNICAL INFORMATION CTR DTIC OCA

2 (PDF) DIRECTOR US ARMY RESEARCH LAB RDRL CIO L IMAL HRA MAIL & RECORDS MGMT

1 (PDF) GOVT PRINTG OFC A MALHOTRA

1 (PDF) DIR USARL WML F B NELSON